

# Classification and control of the origin of photoluminescence from Si nanocrystals

S. GODEFROO<sup>1</sup>, M. HAYNE<sup>1,2\*</sup>, M. JIVANESCU<sup>3</sup>, A. STESMANS<sup>3</sup>, M. ZACHARIAS<sup>4</sup>, O. I. LEBEDEV<sup>5</sup>, G. VAN TENDELOO<sup>5</sup> AND V. V. MOSHCHALOV<sup>1</sup>

<sup>1</sup>INPAC-Institute for Nanoscale Physics and Chemistry, Pulsed Field Group, K.U.Leuven, Celestijnenlaan 200 D, B-3001 Leuven, Belgium

<sup>2</sup>Department of Physics, Lancaster University, Lancaster LA1 4YB, United Kingdom

<sup>3</sup>INPAC-Institute for Nanoscale Physics and Chemistry, Semiconductor Physics Laboratory, K.U.Leuven, Celestijnenlaan 200 D, B-3001 Leuven, Belgium

<sup>4</sup>Institute of Microsystems Engineering, Albert Ludwigs University Freiburg, D-79110 Freiburg, Germany

<sup>5</sup>EMAT, University of Antwerp (RUCA), Groenenborgerlaan 171, 2020 Antwerp, Belgium

\*e-mail: m.hayne@lancaster.ac.uk

Published online: 2 March 2008; doi:10.1038/nnano.2008.7

Silicon dominates the electronics industry, but its poor optical properties mean that III–V compound semiconductors are preferred for photonics applications. Photoluminescence at visible wavelengths was observed from porous Si at room temperature in 1990, but the origin of these photons (do they arise from highly localized defect states or quantum confinement effects?) has been the subject of intense debate ever since. Attention has subsequently shifted from porous Si to Si nanocrystals, but the same fundamental question about the origin of the photoluminescence has remained. Here we show, based on measurements in high magnetic fields, that defects are the dominant source of light from Si nanocrystals. Moreover, we show that it is possible to control the origin of the photoluminescence in a single sample: passivation with hydrogen removes the defects, resulting in photoluminescence from quantum-confined states, but subsequent ultraviolet illumination reintroduces the defects, making them the origin of the light again.

For all its success as an electronic material, Si has one major disadvantage: an indirect bandgap that makes it a poor light emitter. This has given the information age a ‘split personality’<sup>1</sup> in which digital data processing is performed by Si electronics, but increasingly vast amounts of data are transferred optically using photons generated and detected by III–V semiconductors. This problem is likely to become more acute in the near future as the information technology industry moves to optical interconnects for board-to-board and chip-to-chip communications.

The discovery of room-temperature visible photoluminescence (PL) from porous Si in 1990 (refs 2 and 3) increased interest in the optical properties of Si and opened a long-running debate on the origin of PL from porous Si (refs 4 and 5) and, more recently, from Si nanocrystals embedded in SiO<sub>2</sub> (refs 6–11). Besides their potential as light sources<sup>12,13</sup>, it has been shown that Si nanocrystals are strong candidates for a new generation of Flash memory that can be fabricated with minimal disruption to conventional silicon technology<sup>14</sup>.

A consensus has been reached that highly localized defects at the Si/SiO<sub>2</sub> interface<sup>8–10</sup> and the quantum confinement (QC) of excitons<sup>15–17</sup> both play important roles, but it is difficult to experimentally distinguish the mechanisms in the radiative emission<sup>9,10</sup>, especially as the interface-related PL depends on nanocrystal size<sup>8–11</sup>. Here, we report the use of high-field magneto-PL ( $\leq 50$  T) experiments to directly probe the extent of the wavefunction responsible for the PL (refs 18 and 19), and demonstrate that the PL is dominated by defect states. Our results are corroborated by performing electron spin resonance (ESR) measurements, which are used to monitor the presence or absence of (paramagnetic) defects in the sample<sup>20</sup>. We also show

that the origin of the PL can be controlled by using hydrogen passivation to remove the defects, resulting in PL that is due to QC, and ultraviolet (UV) illumination to reintroduce the defects.

## SILICON NANOCRYSTALS AND THEIR DEFECTS

The sample consisted of Si nanocrystals embedded in SiO<sub>2</sub>, and was grown by the deposition of a SiO/SiO<sub>2</sub> superlattice on a Si substrate and subsequent formation of Si nanocrystals in the SiO layers by means of annealing<sup>21</sup>. Transmission electron microscopy (TEM) images show that the annealed sample discussed here consisted of 37 bilayers with thicknesses of 1.5 nm for the layer containing the nanocrystals and 3 nm for the SiO<sub>2</sub> layers. High-resolution TEM (HRTEM) showed that the nanocrystals had an in-plane diameter of  $\sim 3$  nm. Most particles were oblate, with the reduced dimension ( $\sim 1.5$  nm) perpendicular to the layers; others were faceted by (111) planes (Fig. 1). The images clearly show a crystalline Si core (Fig. 1), and this is supported by our ESR data, as well as by previous soft X-ray spectroscopy on similar samples<sup>22</sup>. Less comprehensive experiments were also conducted on five other samples, and gave results that are consistent with those reported here. In particular, it should be noted that the origin of the PL in the as-crystallized state, as determined by magneto-PL, was usually found to be defect-related, but was sometimes due to QC. This variation amongst samples correlated with the defect densities measured using ESR.

The room-temperature PL of the sample in its as-crystallized state is shown in Fig. 2. It consists of a broad gaussian peak centred at 1.61 eV, and is typical of PL from Si nanocrystals. In order to establish the origin of the PL, two types of experiments

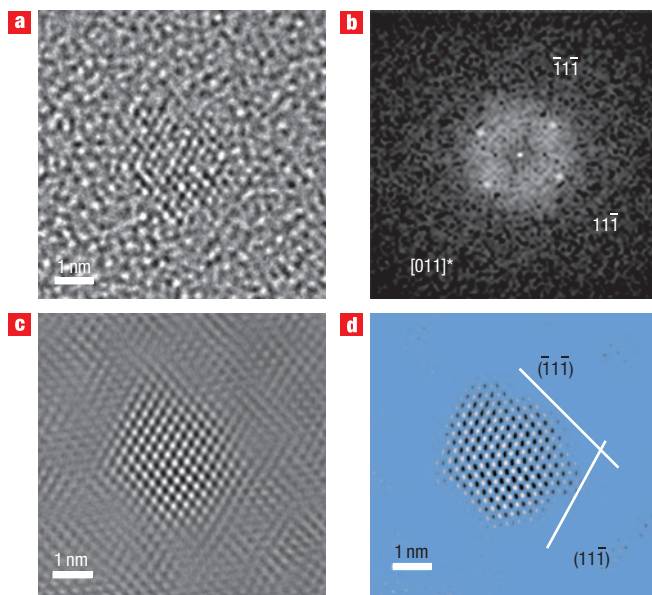


**Figure 1** Imaging of Si nanoparticles by HRTEM. **a**, Image of a single Si nanoparticle along the [011] zone axis. **b**, Corresponding Fourier transform. **c**, Bragg-filtered HRTEM image. **d**, Bragg filtered image after subtraction of the background. This clearly highlights the {111} faceting of this nanoparticle.

were conducted on the sample: ESR and magneto-PL. In the first instance, a high-sensitivity ESR analysis was applied to the sample to quantify the presence of any paramagnetic defects. Two different defect centres were identified (upper spectrum in Fig. 3):  $P_{b(0)}$  (ref. 23) and  $P_{b1}$  (ref. 24). These defects are prototype interface defects characteristic of the Si/SiO<sub>2</sub> interface and are schematically represented in Fig. 3. The presence of  $P_b$ -type defects is important, as these are deep non-radiative recombination centres, which are known to quench the PL from Si nanocrystals in the 1.4–2.2 eV range<sup>15</sup>, irrespective of whether the source of the PL is QC or interface states. The absence of any angle dependence in the  $P_b$  ESR signal indicates that these defects must stem from the interface between the Si nanocrystals and the surrounding SiO<sub>2</sub>, rather than from the Si substrate. From the density of nanocrystals and the inferred density of  $P_b$  defects, we estimate that there is, on average, 1  $P_b$  defect in every 1.4 nanocrystals; that is, at least 30% of the Si nanocrystals are  $P_b$ -defect free, and potentially optically active.

In a second step, the influence of UV irradiation on the defects in the sample was investigated. The sample was irradiated with UV light with a wavelength of  $362 \pm 20$  nm for 71 h, using a 150 W xenon arc lamp and an interference filter. Subsequent to this, the filter was removed from the 150 W xenon arc lamp, and the sample was irradiated with the full UV spectrum centred at 8.2 eV (180–1,000 nm) for 10 h. After each illumination step ESR was performed in order to determine the influence on the defects in the sample. As might be expected, signals from the SiO<sub>2</sub> specific centres  $E'_\gamma$  (ref. 25) and EX (refs 26 and 27) were observed after irradiation with 362 nm UV light, and their intensity increased drastically after irradiation with the full UV spectrum (Fig. 3)<sup>28</sup>. On the other hand, the  $P_{b(0)}$  and  $P_{b1}$  signals did not change within the experimental error of  $\pm 30\%$  after UV irradiation, indicating that there is no hydrogen passivation of the  $P_b$  centres in the as-crystallized sample; that is, they are fully activated. This is

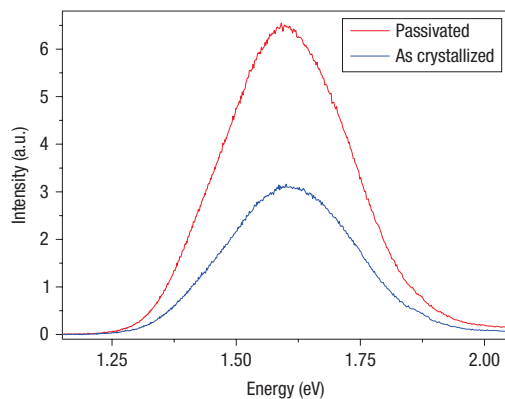


**Figure 2** Room-temperature PL spectra. The spectra were taken under the same experimental conditions for the sample in its as-crystallized (blue line) and passivated (red line) states.

consistent with the sample fabrication procedure, which involved annealing at 1,100 °C in an N<sub>2</sub> atmosphere.

The ESR data demonstrate that the sample has a large number of different defects. None of the defects detected by ESR in the as-crystallized or even in the irradiated sample is PL-active. Nonetheless, this does not prove that the observed PL is from QC, and not from defects. Interface defects that are weakly observed or inactive in ESR can be present, and may even show a Si nanocrystal size dependence, as discussed in references 8–11. For example, Si/SiO<sub>2</sub> defect states that are close to the band edges of the Si nanocrystals, and thus even follow the bandgap widening of Si due to QC, have been reported<sup>8</sup>. In such defects, the PL is initiated by interband carrier excitation in the Si nanocrystals, followed by relaxation to the interface defect states (Fig. 4). The transition to the lower-energy interface defect state is radiative, with a PL energy close to the one determined from QC (ref. 8). However, the aim here is not to identify the microscopic origin of interface-defect PL in Si/SiO<sub>2</sub>, but to unambiguously demonstrate that we can distinguish between QC and defect PL in Si/SiO<sub>2</sub> nanostructures using a high magnetic field, and that we can switch between the two sources of PL in a single sample.

## ORIGIN OF THE PHOTOLUMINESCENCE

To determine the origin of the luminescence, PL measurements were performed at 85 K in pulsed magnetic fields  $B$  up to 50 T on the as-crystallized sample (that is, before UV irradiation). The principle behind such experiments is quite straightforward—the applied magnetic field has an associated length scale, the magnetic length  $\ell = \sqrt{\hbar/eB}$ , where  $\hbar$  is the reduced Planck constant and  $e$  is the electron charge, which acts to confine the wavefunction of the state under study before recombination, and hence increases the PL energy. Clearly, the smaller the extent of the wavefunction, the smaller the diamagnetic shift of the centre of mass of the PL,  $\Delta E_{\text{CM}}$ . Indeed, in the low-field limit, where  $\ell$  is large compared to the wavefunction extent<sup>18,19,29</sup>,

$$\Delta E_{\text{CM}} = \frac{e^2 \langle \rho^2 \rangle}{8\mu} B^2, \quad (1)$$

where  $\mu$  is the reduced effective mass and  $\langle \rho^2 \rangle^{1/2}$  is the average wavefunction extent in the plane perpendicular to the applied field. Thus, such an experiment should be able to unequivocally

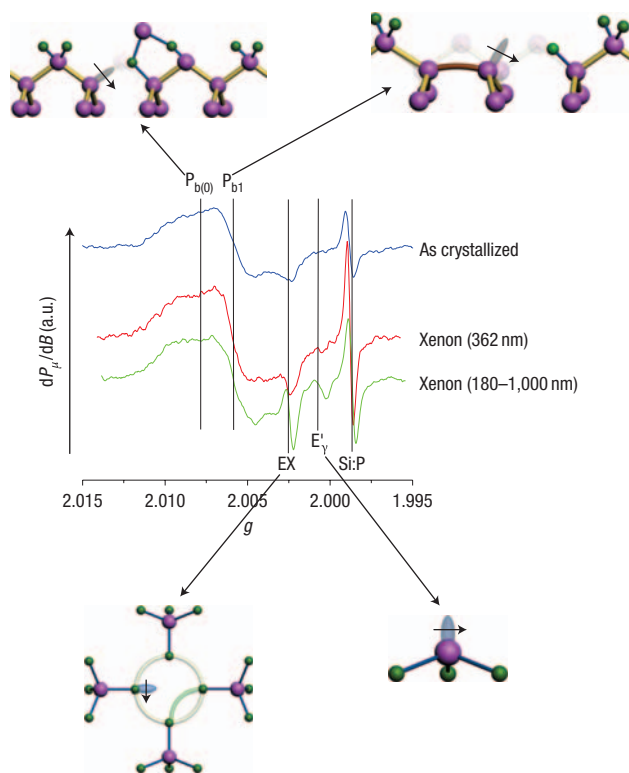


**Figure 3** ESR spectra at 4.2 K The upper spectrum is in the as-crystallized state, the middle spectrum after xenon arc lamp illumination at  $\sim 362$  nm, and the lower spectrum after unfiltered xenon arc lamp irradiation. In total, four different defects are identified:  $P_{b(0)}$ ,  $P_{b1}$ ,  $E_v$  and EX, which are also schematically represented. The purple and green spheres represent the Si and O atoms, respectively. The arrows in the schematics depict the unpaired electrons and the brown Si–Si bond indicates the strained bond. The signal Si:P is a marker from an added reference sample.

distinguish between a state confined to a few nanometres within a Si nanocrystal and a highly localized defect state. However, such experiments are not trivial to perform in practice. The laser light and PL are transmitted to and from the magnet and cryostat using optical fibres, which also show a PL signal at a similar energy to that of the sample as a result of UV absorption in the fibres. This necessitates the use of special procedures to eliminate this background (see Methods). Second, the sample signal is relatively weak compared with III–V semiconductor nanostructures, and requires the use of a state-of-the-art charge-coupled-device detector capable of single-photon detection in order to count sufficient photons in the 5-ms integration time. For the same reason it was only possible to obtain a single spectrum at the peak field of each 25-ms magnetic-field pulse. Finally, the expected diamagnetic shift of the PL at 50 T is expected to be extremely small, even for QC:  $\sim 0.5\%$  of the full-width at half-maximum (FWHM) of the PL (300 meV). In order to detect such small changes in the PL energy in an experiment that involves making a series of pulses for each field value over the period of a day, the zero-field peak position was measured before and after every pulse to eliminate any effects of drift over time in the apparatus, and to reduce the effects of heating from the pulse and mechanical realignment. As a result we defined  $\Delta E_{CM}$  as the difference in energy of the PL at the peak of the pulse and the average of the two zero-field values taken before and after the pulse. The result is plotted in Fig. 5a for the

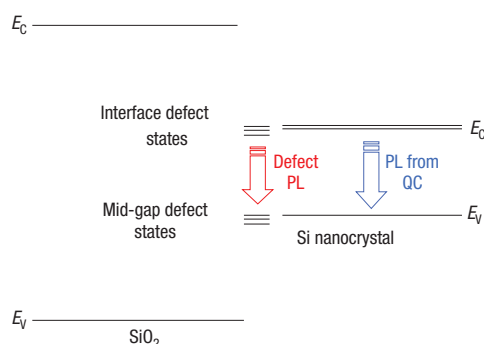


**Figure 4** Band structure and competing PL mechanisms for Si nanocrystals embedded in  $\text{SiO}_2$ . The bandgap of  $\text{SiO}_2$  is 8.8 eV, and the bandgap of Si increases from the bulk value of 1.12 eV to 1.6–2.6 eV for Si nanocrystals due to QC. There are two different bands of defect states: the interface defect states close to the conduction band ( $E_c$ ) of Si and the mid-gap defect states with energies close to the valence band ( $E_v$ ) of Si. The conduction band of the Si nanocrystal has two sub-levels (explained in ref. 8).

as-crystallized sample. It can be seen that the shift, if any, is very small. As there is a slight hint of a very small shift, it is not possible to exclude a small contribution to the PL from QC. Nonetheless, it is clear that in the as-crystallized state the PL is completely dominated by PL from highly localized defect states.

This conclusion appears to contradict previous work that has cited the observation of phonon replica as proof of QC in ensemble studies of samples similar to those studied here<sup>30</sup>. On the other hand, in single dot measurements of Si nanocrystals formed in etched nanopillars<sup>31</sup>, an acoustic phonon replica at 6 meV was always observed, whereas optical phonon replica were only observed for approximately 1 in 3 of the dots. This was noted as being somewhat unexpected, and tentatively attributed to the carriers being ‘strongly localized’ in some nanocrystals. (A highly localized state has a small dipole and so will couple weakly to optical phonons.) Clearly, the question of phonon replica associated with defect states needs further investigation.

In the next step, we passivated the sample in 1 atm of pure hydrogen for 30 min at a temperature of 400 °C. This temperature does not influence the size and nature of the Si nanocrystals because the formation of amorphous Si clusters needs temperatures in excess of 600 °C, and crystallization of amorphous Si clusters only appears above 900 °C (ref. 32). We then repeated the ESR and PL measurements. The zero-field PL and ESR spectra are shown in Figs 2 and 6a, respectively. First, it can be seen that the passivation has had a remarkable effect on the ESR signal (Fig. 6a). All traces of any defects have been removed, the only part that remains being the Si:P marker signal. Second, the intensity of the PL signal has increased, consistent with the removal of the  $P_b$  defects. Assuming that the passivation has also eliminated the ESR-inactive defects, we can suppose that the PL is now of entirely QC origin. This can be clearly seen in the data from a second magneto-PL experiment (Fig. 5b): A parabolic shift of about 1.5 meV is observed. Using an estimated reduced mass of  $0.20m_0$  ( $m_0$  is the free electron mass), obtained by assuming an isotropic electron mass of  $0.33m_0$  and a heavy hole mass of  $0.54m_0$  (ref. 33), a wavefunction extent of  $4.9 \pm 0.1$  nm in the plane of the sample is found. This is somewhat bigger than the diameter of 3 nm measured from HRTEM, and may result from the fact that the transition from Si to  $\text{SiO}_2$  occurs through a sub-oxide layer, resulting in some leakage of the confined wavefunction out of the nanocrystal<sup>22</sup>.

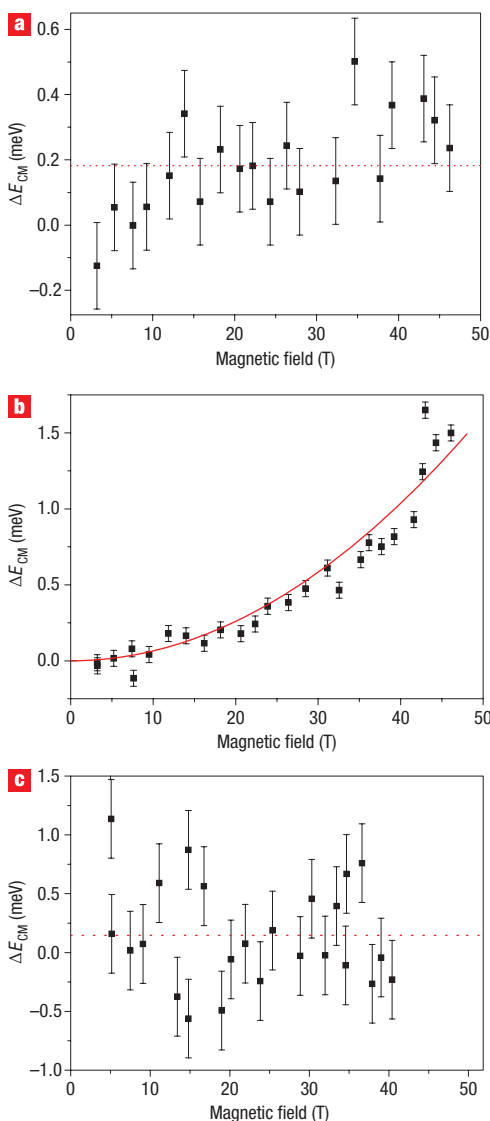


**Figure 5** Shift of the centre of mass of the PL peak ( $\Delta E_{\text{CM}}$ ) as a function of magnetic field at 85 K. The error bars are the mean of the absolute difference in centre of mass of 0 T spectra taken before and after each field pulse. **a**, Data for the as-crystallized sample. The dotted line indicates the mean value of  $\Delta E_{\text{CM}}$ . **b**, After passivation the solid line shows the parabolic fit. **c**, Data after passivation and subsequent UV irradiation at room temperature. The dotted line is the mean value. A clear parabolic field dependence, such as is observed in **b**, is characteristic of a PL from a state that is quantum confined by the nanocrystal, whereas no detectable field dependence indicates that a very highly localized (defect) state is responsible for the PL (**a** and **c**). The error bars in **b** are much smaller than in **a** or **c** due to the increased intensity of the signal.

## REINTRODUCING THE DEFECTS

Having demonstrated the origin of the PL as defects in the as-crystallized state and QC after passivation, we then went on to reintroduce the defects using UV illumination from an Ar<sup>+</sup> laser (351–364 nm radiation). Two experiments were conducted. First, the whole surface of a piece of passivated sample was irradiated at room temperature by a defocused beam for almost 330 h. The effect on the ESR spectrum is shown in Fig. 6a. The irradiation has reactivated the P<sub>b</sub> and E<sub>y</sub>' centres, although the density of

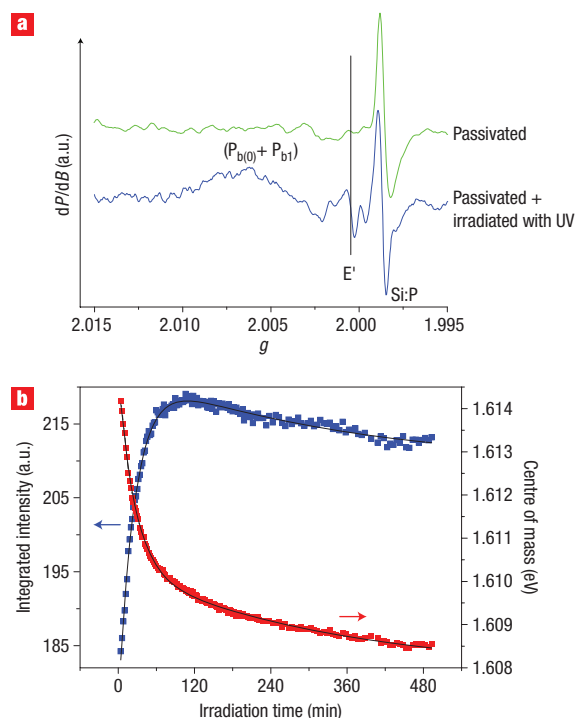


**Figure 6** Effect of UV irradiation on a passivated sample. **a**, ESR spectra at 4.2 K for the passivated sample (upper spectrum) and after subsequent UV irradiation (lower spectrum). It can be seen that passivation removes the defects (the only remaining signal is the Si:P marker), and that UV irradiation reintroduces them. **b**, Time dependence of the centre of mass (right-hand axis) and integrated intensity (left-hand axis) of the PL, after passivation and during irradiation with the UV lines of an unfocused Ar<sup>+</sup> laser. The lines are fits to the data using double exponential functions.

defects is substantially less than for the as-crystallized sample. In the second experiment another piece of passivated sample was irradiated at room temperature by an unfocused Ar<sup>+</sup> laser beam over a period of 8 h, and PL spectra were taken at regular intervals. It is estimated that the accumulated doses of UV radiation received in the two experiments are similar, but our conclusions are not dependent on the two treatments being equivalent. The integrated intensity and centre of mass of the PL are shown in Fig. 6b as a function of irradiation time with the unfocused laser beam. It can be seen that both curves have a 'fast' and a 'slow' component. The intensity initially rapidly increases, and then after about 2 h starts to decrease. The centre of mass shows a strong redshift, followed by a weaker dependence after the same 2-h period. Indeed, both curves can be fitted with a double exponential function, yielding the same two time constants in both cases: 26 min for the 'fast' component and 337 min for the 'slow' component. This implies that the observed behaviour is the result of two competing effects. As we know from ESR that UV illumination introduces or reactivates defects due to the Stäbler–Wronski effect<sup>34</sup>, we attribute the first mechanism, which increases the PL intensity, to the reactivation of the interface defects responsible for the PL in the as-crystallized sample. This explanation is consistent with the observed redshift, as such defects emit PL at an energy that is slightly lower than that of QC (ref. 8). For the same reason we can expect that the reactivation of the defect PL in any particular nanocrystal will quench the QC PL, especially if carrier relaxation

from the Si conduction band to interface defect states (Fig. 4) is faster than the recombination time. The second effect, with a much slower time constant, decreases the PL intensity, and is therefore very likely to be the result of the reactivation of  $P_b$  defects in the Si nanocrystals, because they quench the PL and are known to reappear as a result of illumination with the UV lines of the  $Ar^+$  laser (Fig. 6a). The corresponding redshift of the PL can be attributed to the preferential reactivation of defects in smaller nanocrystals that emit at higher energies, as these will tend to be more strained. The net effect is that illumination with UV light reverses the effect of passivation, and we return to interface defects as the origin of the PL. Note that H is immobile in the sample at 85 K, thus the UV illumination during the magneto-PL experiments does not affect the defects.

As the time constant of the fast component in Fig. 6b is 26 min, illumination for 8 h should result in 95% of the interface defects being reactivated. Although their PL may still be quenched by the reintroduction of  $P_b$ -type defects, we can reasonably expect that after illumination the PL is, once again, totally of interface-defect origin. Figure 5c shows  $\Delta E_{CM}$  versus magnetic field for the sample that was passivated and subsequently irradiated with a defocused laser beam. Although the data are somewhat noisy, it is evident that there is no diamagnetic shift, entirely confirming our expectations: the PL is of defect-related origin again.

In summary, we have shown that high magnetic fields can be used to unambiguously classify the origin of PL from Si nanocrystals in  $SiO_2$  as either from defects or QC. We have further shown that by a combination of passivation to remove defects and UV irradiation to reintroduce them, we can switch from defect-related PL, to QC PL, and back again to defect-related PL in a single sample.

## METHODS

### SUPERLATTICE APPROACH

An amorphous  $SiO/SiO_2$  superlattice was grown by reactive evaporation of SiO powders in an oxygen atmosphere. The films were deposited on 4-inch wafers with a substrate temperature of 100 °C. Rotation of the substrate enabled high homogeneity over the whole wafer. The Si nanocrystals were then formed by phase separation during thermal annealing at 1,100 °C for 1 h under an  $N_2$  atmosphere:  $2SiO \rightarrow SiO_2 + Si$ . This growth method allowed the independent control of crystal size and density, and the Si nanocrystals were separated by a thin oxide shell<sup>21</sup>.

### ELECTRON SPIN RESONANCE

Conventional first-order absorption-derivative ( $dP_\mu/dB$ ) ESR was measured using a K-band spectrometer operating at a frequency of ~20.5 GHz, equipped with a  $TE_{011}$  cavity. For reasons of sensitivity, all spectra were taken at 4.2 K. The measurements were performed with the amplitude of the applied sinusoidal modulation of the magnetic field (~100 kHz) and incident microwave power properly adjusted so that the measured signals were not visibly distorted. In order to improve the signal-to-noise ratio for each spectrum, 100 scans were typically accumulated. For ESR signal intensity and g factor calibration, a Si:P marker sample was identically co-mounted with the Si nanocrystal sample for each measurement. To obtain the absolute values of the defect densities, the double numerical integration of the detected derivative absorption spectrum was compared with that of the marker, both recorded in the same trace. Generally, measurements were carried out with the applied magnetic field  $B \parallel n$ , the (100) Si substrate normal. The signal anisotropy was checked by varying the angle ( $\varphi_B$ )  $B$  makes with  $n$ .

### PHOTOLUMINESCENCE IN PULSED MAGNETIC FIELDS

To conduct PL measurements in high magnetic fields, optical fibres were used to bring the laser light to the sample. For the measurements discussed here, a long (25 m) and a short (2 m) excitation fibre were used with a bandpass filter between. The emitted light was transferred to the detector through a bundle of 7 detection fibres, 25 m in length. Because of the low PL intensity, an exposure time of 5 ms was needed and only one spectrum could be taken during a 25-ms magnetic field pulse. The exposure time was chosen at the peak of the pulse in

such a way that the standard deviation of the magnetic field while counting photons was less than 5%. The plane of the sample was mounted at an angle of 8° to the plane perpendicular to the applied field, and the excitation fibre was placed at an angle of 11° with respect to the collection fibres, which were parallel to the applied field, in such a way as to make an angle of 19° between the laser excitation and PL detection fibres. This was done to reduce the reflection of the UV laser light into the detection fibres. Further details on the magneto-PL technique and its application to semiconductor nanostructures can be found in reference 19.

Received 17 December 2007; accepted 4 February 2008;  
published 2 March 2008.

## References

- Ball, P. Let there be light. *Nature* **409**, 974–976 (2001).
- Canham, L. T. Silicon quantum wire array fabrication by electrochemical and chemical dissolution of wafers. *Appl. Phys. Lett.* **57**, 1046–1048 (1990).
- Lehmann, V. & Gösele, U. Porous Si formation: A quantum wire effect. *Appl. Phys. Lett.* **58**, 856–858 (1991).
- Fauchet, P. M. Photoluminescence and electroluminescence from porous silicon. *J. Lumin.* **70**, 294–309 (1996).
- Wolkin, M. V. *et al.* Electronic states and luminescence in porous Si: The role of oxygen. *Phys. Rev. Lett.* **82**, 197–200 (1999).
- Hadjisavvas, G. & Kelires, P. C. Theory of interface structure, energetics, and electronic properties of embedded Si/a- $SiO_2$  nanocrystals. *Physica E* **38**, 99–105 (2007).
- Heitmann, J., Müller, E., Zacharias, M. & Gösele, U. Silicon nanocrystals: Size matters. *Adv. Mater.* **17**, 795–803 (2005).
- Averboukh, B. *et al.* Luminescence studies of a Si/ $SiO_2$  superlattice. *J. Appl. Phys.* **92**, 3564–3568 (2002).
- Puzder, A., Williamson, A. J., Grossman, J. C. & Galli, G. Surface chemistry of silicon nanoclusters. *Phys. Rev. Lett.* **88**, 097401 (2002).
- Hadjisavvas, G. & Kelires, P. C. Structure and energetics of Si nanocrystals embedded in a- $SiO_2$ . *Phys. Rev. Lett.* **93**, 226104 (2004).
- Wang, X. X. *et al.* Origin and evolution of photoluminescence from Si nanocrystals embedded in a  $SiO_2$  matrix. *Phys. Rev. B* **72**, 195313 (2005).
- Pavesi, L., Dal Negro, L., Mazzoleni, C., Franzo, G. & Priolo, F. Optical gain in silicon nanocrystals. *Nature* **408**, 440–444 (2000).
- Walters, R. J., Bourianoff, G. I. & Atwater, H. A. Field-effect electroluminescence in silicon nanocrystals. *Nature Mater.* **4**, 143–146 (2005).
- Tiwari, S. *et al.* A silicon nanocrystal based memory. *Appl. Phys. Lett.* **68**, 1377–1379 (1996).
- Deleerue, C., Allan, G. & Lannoo, M. Theoretical aspects of the luminescence of porous silicon. *Phys. Rev. B* **48**, 11024–11036 (1993).
- Delley, B. & Steigmeier, E. F. Quantum confinement in Si nanocrystals. *Phys. Rev. B* **47**, 1397–1400 (1993).
- Ogüt, S., Chelikowsky, J. R. & Louie, S. G. Quantum confinement and optical gaps in Si nanocrystals. *Phys. Rev. Lett.* **79**, 1770–1773 (1997).
- Hayne, M. *et al.* Electron and hole confinement in stacked self-assembled InP quantum dots. *Phys. Rev. B* **62**, 10324–10328 (2000).
- Hayne, M. *et al.* Pulsed magnetic fields as probe of self-assembled semiconductor nanostructures. *Physica B* **346–347**, 421–427 (2004).
- Poindexter, E. H. & Caplan, P. J. Characterization of Si/ $SiO_2$  interface defects by electron spin resonance. *Prog. Surf. Sci.* **14**, 201–294 (1983).
- Zacharias, M. *et al.* Size-controlled highly luminescent silicon nanocrystals: A SiO/ $SiO_2$  superlattice approach. *Appl. Phys. Lett.* **80**, 661–663 (2002).
- Zimina, A. *et al.* Electronic structure and chemical environment of silicon nanoclusters embedded in a silicon dioxide matrix. *Appl. Phys. Lett.* **88**, 163103 (2006).
- Stesmans, A. & Afanas'ev, V. V. Electron spin resonance features of interface defects in thermal (100)Si/ $SiO_2$ . *J. Appl. Phys.* **83**, 2449–2457 (1998).
- Stesmans, A., Nouwen, B. & Afanas'ev, V. V.  $P_{b1}$  interface defect in thermal (100)Si/ $SiO_2$ :  $^{17}O$  hyperfine interaction. *Phys. Rev. B* **58**, 15801–15809 (1998).
- Warren, W. L., Poindexter, E. H., Offenber, M. & Müller-Warmuth, W. Paramagnetic point defects in amorphous silicon dioxide and amorphous silicon nitride thin films. *J. Electrochem. Soc.* **139**, 872–880 (1992).
- Stesmans, A. & Scheerlinck, F. Generation aspects of the delocalized intrinsic EX defect in thermal  $SiO_2$ . *J. Appl. Phys.* **75**, 1047–1058 (1994).
- Stesmans, A. & Scheerlinck, F. Natural intrinsic EX center in thermal  $SiO_2$  on Si:  $^{17}O$  hyperfine interaction. *Phys. Rev. B* **50**, 5204–5212 (1994).
- Tsai, T. E., Griscom, D. L. & Friebele, E. J. Mechanism of intrinsic Si E'-center photogeneration in high-purity silica. *Phys. Rev. Lett.* **61**, 444–446 (1988).
- Walck, S. N. & Reinecke, T. L. Exciton diamagnetic shift in semiconductor nanostructures. *Phys. Rev. B* **57**, 9088–9096 (1998).
- Heitmann, J. *et al.* Excitons in Si nanocrystals: Confinement and migration effects. *Phys. Rev. B* **69**, 195309 (2004).
- Sychugov, I., Juhász, R., Valenta, J. & Linnros, J. Narrow luminescence linewidth of a silicon quantum dot. *Phys. Rev. Lett.* **94**, 087405 (2005).
- Yi, L. X., Heitmann, J., Scholz, R. & Zacharias, M. Si rings, Si clusters, and Si nanocrystals—different states of ultrathin  $SiO_2$  layers. *Appl. Phys. Lett.* **81**, 4248–4250 (2002).
- Davies, J. H. *The Physics of Low-Dimensional Semiconductors* (Cambridge Univ. Press, Cambridge, UK, 1998).
- Abtew, T. A. & Drabold, D. A. Atomistic simulation of light-induced changes in hydrogenated amorphous Si. *J. Phys. Condens. Matter* **18**, L1–L6 (2006).

## Acknowledgements

This work was supported by the SANDiE Network of Excellence of the European Commission (NMP-CT-2004-500101), the Belgian Inter-University Attraction Pole, Flemish Geconcerteerde Onderzoeksaacties and Fonds voor Wetenschappelijke Onderzoek programma's and project ZA191/14-3 of the German Research Foundation (DFG). M.H. is an Academic Fellow of the Research Councils UK. Correspondence and requests for materials should be addressed to M.H.

Reprints and permission information is available online at <http://npg.nature.com/reprintsandpermissions/>